

THE SCIENCE AND TECHNOLOGY OF VAPOR PHASE PROCESSING AND MODIFICATION OF SURFACES

A diffusion approach for plasma synthesis of superhard tantalum borides

Aaditya Rau¹, Kallol Chakrabarty², William Gullion³, Paul A. Baker², Ilias Bikmukhametov⁴, Richard L. Martens⁵, Gregory B. Thompson⁴, Shane A. Catledge^{2,a)}

Received: 31 July 2019; accepted: 8 November 2019

Microwave plasma chemical vapor deposition (MPCVD) was used to diffuse boron into tantalum using plasma initiated from a feedgas mixture containing hydrogen and diborane. The role of substrate temperature and substrate bias in influencing surface chemical structure and hardness was investigated. X-ray diffraction shows that increased temperature results in increased TaB2 formation (relative to TaB) along with increased strain in the tantalum body-centered cubic lattice. Once the strained tantalum becomes locally supersaturated with boron, TaB and TaB2 precipitate. Additional boron remains in a solid solution within the tantalum. The combination of precipitation and solid solution hardening along with boron-induced lattice strain may help explain the 40 GPa average hardness measured by nanoindentation. Application of negative substrate bias did not further increase the hardness, possibly due to etching from increased ion bombardment. These results show that MPCVD is a viable method for synthesis of superhard borides based on plasma-assisted diffusion.

Introduction

Downloaded from https://www.cambridge.org/core. IP address: 24.96.9.145, on 07 Apr 2020 at 20:06:57, subject to the Cambridge Core terms of use, available at https://www.cambridge.org/core/terms. https://doi.org/10.1557/imr.2019.35

Metal borides have long been a subject of interest due to their desirable properties [1], such as increased hardness, wear resistance, and chemical stability [2]. Of these compounds, borides of tantalum have come into the focus due to their excellence in these properties [3]. Specifically, these properties include high hardness, high mechanical strength and wear resistance, high melting point, chemical stability, and high electrical and thermal conductivity. As a result, tantalum borides are a good candidate in high-temperature mechanical applications, in application as hard refractory materials and as conducting components with good wear and corrosion resistance [4].

A wide variety of techniques have been used to synthesize tantalum borides, including traditional powder or pack boriding [5], high temperature/pressure compression in diamond

anvil cells [6, 7], and chemical vapor deposition (CVD) using tantalum-based precursors [8]. However, these methods are not without drawbacks. In pack boriding, studies have found that the powder used often leaves contaminants within the boride, which may be undesirable [5]. Diamond anvil cells are typically only able to produce small volumes of usable material. Sintering of tantalum boride powders into ceramics requires conditions of high pressure and temperature [7] in order to be effective. CVD can be used to produce discrete tantalum boride coatings [8], but stress gradients at the coating/substrate interface may result in poor adhesion, therefore precluding some applications. Furthermore, CVD precursors for tantalum, such as TaCl₅, require extra handling (such as sublimation from a powder source) to contain reactants and may pose implementation challenges [9].

In this work, we rely on microwave plasma CVD (MPCVD) to diffuse boron into tantalum substrates using a hydrogen-rich feedgas mixture containing only 0.12% of diborane. An advantage of the microwave plasma is the

¹Department of Mechanical Engineering, Whiting School of Engineering, The Johns Hopkins University, Baltimore, Maryland 21218-2682, USA ²Department of Physics, Center for Nanomaterials and Biointegration (CNMB), The University of Alabama at Birmingham, Birmingham, Alabama 35394-1170, USA

³Department of Physics, Brigham Young University—Idaho, Rexburg, Idaho 83460, USA

⁴Department of Metallurgical & Materials Engineering, The University of Alabama, Tuscaloosa, Alabama 35487, USA

⁵Alabama Analytical Research Center, Tuscaloosa, Alabama 35487, USA

^{a)}Address all correspondence to this author. e-mail: catledge@uab.edu

^{&#}x27;A previous error in this article was corrected, please see doi:10.1557/jmr.2019.400.

Downloaded from https://www.cambridge.org/core. IP address: 24.96.9.145, on 07 Apr 2020 at 20:06:57, subject to the Cambridge Core terms of use, available at https://www.cambridge.org/core/terms. https://doi.org/10.1557/jmr.2019.357



efficient creation of excited-state atomic boron and BH species that detectable at 249 nm and 433 nm, respectively, via optical emission spectroscopy (OES). The method of CVD boron diffusion into a tantalum substrate differs from the conventional approach that uses a gas-phase reaction between both tantalum- and boron-based precursors to deposit metal borides as a discrete coating onto a substrate [8]. By instead relying solely on diffusion of boron into the substrate, we avoid tantalum-containing precursors (e.g., TaCl₄) that are challenging to implement or that may cause contamination in the coating structure. In addition, the nature of CVD affords the opportunity to discover new structures that are not likely to occur under equilibrium pressure and temperature conditions. Notably, our previous work on CoCrMo and WC-Co plasma borides finds that a mix of boride phases forms after CVD processing [10, 11]. The presence of phase mixtures may allow for hardening mechanisms, including solid solution and precipitation hardening, to further increase hardness of the tantalum boride layer beyond that expected from a simple rule of mixture estimation. Our goal is to create novel superhard tantalum borides via a CVD boron diffusion process. This process allows a seamless transition from superhard surface to bulk metal, avoiding discrete interfaces that could act as a driving force for coating delamination. Our previous work on plasma boriding of other metals and metal alloys [10, 11, 12] has consistently shown improvements in hardness and/or has made the surface more amenable to further treatments. Reports of postdeposition annealing [13, 14] (such as from magnetron sputter-deposited TiN/CrAlN films) reveal that grain size increases with annealing temperature whereas the hardness of the film decreases. However, the hardness of such films was found to increase with an applied substrate bias voltage [15]. The high hardness of the film at low temperature and higher bias voltage can be explained as originating from a dense structure with small grain size and large internal stress. This, in turn, is caused by increased bombardment of highly energetic particles from the applied bias voltage. In the current study, we independently vary two growth parameters, substrate temperature, and substrate bias, in order to understand how these factors affect the structure and hardness of the plasma-borided tantalum. Application of a negative direct current (DC) bias voltage to the substrate may further increase hardness associated with ion bombardment mechanisms at the growing surface [16].

Results and discussion

Effect of substrate temperature

Processing conditions for all samples are summarized in Table I. For the nonbias samples (A, B, and C), the surfaces after plasma boriding were at least partially covered by a discrete dark coating. In some cases, this discrete coating

TABLE I: Sample ID and deposition conditions.

Sample ID	Forward power/reflected power (W)	Approximately average temperature (°C)	Applied bias (V)
A	600/50	700	0
В	700/50	775	0
C	1000/20	850	0
D	600/80	800	-50
E	600/30	800	-150
F	600/40	750	-250
G	600/50	775	-350

could be removed during cleaning with acetone and isopropanol. The extent of coverage of this coating was significantly reduced for higher substrate temperature (sample C). X-ray photoelectron spectroscopy (XPS) of the discrete coating revealed a boron-rich surface (>75%), with relatively small amounts of carbon (8-13%) and oxygen (5-8%). However, both oxygen and carbon signals disappeared with sputtering, suggesting they were adventitious in origin. As shown in the scanning electron microscopy (SEM) images of Fig. 1, the regions of dark contrast appear as a discrete coating on the surface while the remaining regions of light contrast resemble the original substrate (no coating). Higher magnification of the dark-contrast regions (not shown) reveals dense submicron spherical nodules. For samples grown at higher substrate temperature, less dark coating formed with less continuity, as shown for sample B in Fig. 1(b). A highmagnification image of the noncoated region of sample B is shown in Fig. 1(c) and its appearance resembles bare metal. For sample A (made at 700 °C), the dark coating covers most of the surface while for sample C (made at 850 °C, not shown), the vast majority of the borided sample surface resembled bare metal. The increase of substrate temperature is expected to enhance the diffusion of boron into the substrate, minimizing boron saturation on the surface where it otherwise forms as a boron-rich coating.

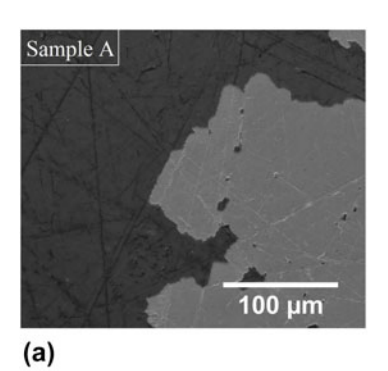
Optical pyrometry can give insight into the diffusion process. When a discrete coating forms, the substrate temperature (as measured by the pyrometer) oscillates with increasing growth time, indicating rate of growth [17]. We find that increasing temperature correlates with a larger period of oscillation suggesting that less coating forms in the given processing time. The formation and extent of the discrete dark coating was found to decrease with increasing substrate temperature, as shown in Fig. 1. Therefore, in situ oscillatory pyrometry data may be an indicator of the effectiveness of the diffusion process, i.e., revealing the degree to which boron is diffused into the material or is accumulated on the surface as a discrete coating.

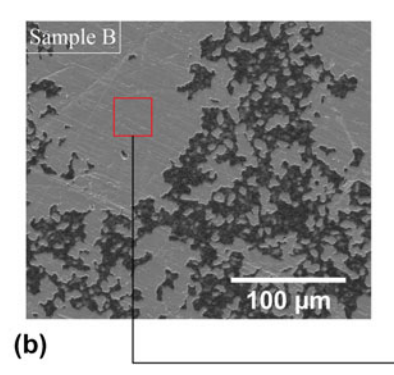
📗 Journal of Materials Research 📗 Volume 35 📄 Issue 5 🖿 Mar 16, 2020 📄 www.mrs.org/jm

482

In order to understand the effect of substrate temperature on surface phase structure, samples were analyzed by glancing-angle X-ray diffraction (XRD). The diffraction patterns of samples A, B, and C, are shown in Fig. 2. The patterns show that for increasing substrate temperature (samples A–C), reflections from the body-centered cubic (BCC) Ta and







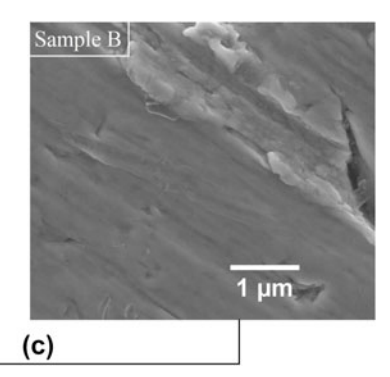


Figure 1: SEM images of (a) sample A (700 °C) showing the dark boron-rich discontinuous coating along with a lighter-contrast region associated with the borondiffused substrate, (b) sample B (775 °C) showing the more pronounced discontinuity of the coating for increased substrate temperature, and (c) sample B zoomed on an area (red square) from the boron-diffused substrate surface, where superhard values were found.

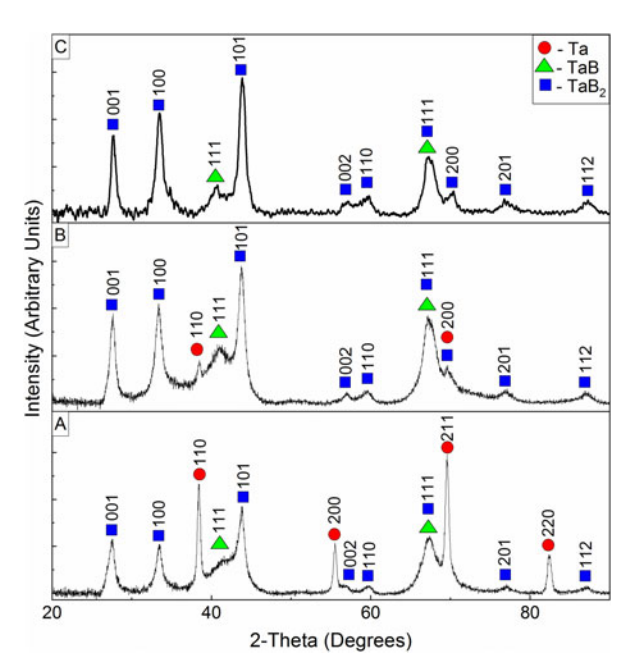


Figure 2: XRD scans for samples A, B, and C with peaks indexed to Ta, TaB, and TaB₂ structures.

orthorhombic TaB phases decrease in intensity while reflections from the hexagonal TaB2 phase increase in intensity.

These patterns also support the expectation that diffusion of boron is enhanced at higher substrate temperature, with higher temperature leading to more development of the TaB₂ phase over the TaB phase. The lattice constants from the Rietveld fit for each sample are presented in Table II. Notably, BCC Ta shows an increase in unit cell volume with increasing temperature from samples A to B (note that no Ta peaks could be detected in sample C due to the larger thickness of the boride layer). The increase in Ta unit cell volume with temperature is consistent with higher boron diffusion into the lattice. Lattice strain in the near-surface was estimated from the measured lattice parameter for the BCC tantalum unit cell. The majority of this lattice strain in Ta is presumed to be caused by boron incorporation as a solid solution. The stress is calculated as the product of measured tantalum Young's modulus (E) \times BCC tantalum lattice strain (ϵ), from E = σ/ϵ . Boron likely forms a solid solution in tantalum and the resulting tensile lattice strain is measured to be 0.27% for sample A and 3.4% for sample B. Given the measured Young's modulus for bare tantalum metal of 190 GPa, the calculated tensile stress in the tantalum is 0.51 GPa (sample A) and 6.5 GPa (sample B). The hexagonal close packed (HCP) TaB2 unit cell c-axis for each sample A-C is consistently shortened compared to the standard (inorganic crystal structure database, ICSD), resulting in a cell volume that remains compressed compared to the standard. The transition from compressive to tensile stress (from surface to bulk) for hard ceramic materials on ductile metals processed at elevated temperatures is not uncommon and is predicted based on the differences in thermal expansion between the two materials [18, 19]. Since our borides made at elevated temperature (e.g., sample C) are not deposited as a discrete coating, stresses generated within the boride phase (compressive) and within the Ta-B solid solution (tensile) can likely be sustained without stress-induced damage of the surface.

Nanoindentation was used to measure hardness of the borided samples. Testing was performed on the metalliclooking regions of the samples where boron is presumed to be diffused into the metal, e.g., see Fig. 1(c). Histograms of hardness values for samples A, B, and C are given in Fig. 3(a), where *n* is the number of data points, μ is the mean, and σ is the standard deviation.

The difference in average hardness from sample A (11.8 \pm 7.1 GPa) to sample B (41.7 \pm 11.5 GPa) is large and significant. The lower mean hardness in sample A may be a result of a relatively thin boride layer, which could have caused the indenter measurements to be influenced by the underlying bulk of the Ta substrate. This is supported by XRD (Fig. 2), which shows significantly more Ta signal, relative to TaB and TaB2, for sample A compared to samples B and C. For 150-nm



Downloaded from https://www.cambridge.org/core. IP address: 24.96.9.145, on 07 Apr 2020 at 20:06:57, subject to the Cambridge Core terms of use, available at https://www.cambridge.org/core/terms. https://doi.org/10.1557/jmr.2019.357

TABLE II: Lattice constants for each phase structure found via the Rietveld refinement.

Compound	Standard ^a	Sample A	Sample B	Sample C	Sample D	Sample E	Sample F	Sample G
	(a, b, c) (Å)	(a, b, c) (Å)	(a, b, c) (Å)	(a, b, c) (Å)	(a, b, c) (Å)	(a, b, c) (Å)	(a, b, c) (Å)	(a, b, c) (Å)
Ta (BCC)	3.296	3.3048	3.4079	(No Ta reflections)	(No Ta reflections)	3.3047	3.3067	(No Ta reflections)
TaB (ortho-	3.270, 8.854,	3.3242, 8.675,	3.2722, 8.8178,	3.2400, 9.0005,	3.2391, 8.9455,	3.2662, 8.7863,	3.3093, 8.656,	3.2262, 8.9136,
rhombic)	3.154	3.4249	3.1494	3.1605	3.2088	3.2042	3.2437	3.2691
TaB ₂ (HCP)	3.098, 3.240	3.089, 3.232	3.0981, 3.2347	3.1048, 3.2332	3.111, 3.2421	2.8633, 3.2945	3.0925, 3.2354	3.1136, 3.242

Ta (reference code: 98-015-1407); TaB (reference code: 98-018-6194); TaB₂ (reference code: 96-151-0839).

indentation depth, the mean hardness value for sample B (41.7 \pm 11.5 GPa) and sample C (39.0 \pm 12.3 GPa) is comparable and not statistically different. Both of these samples show a large distribution in hardness, with some values exceeding 70 GPa. From load versus displacement data of softer regions, the loading curve often exhibits a "pop-in" discontinuity that can be indicative of porosity or material processes (e.g., crack or dislocation formation, phase transformation, and strain transfer across grain boundaries, etc.) within the indentation interaction volume. In contrast, when the indenter measures a very hard region, the load versus displacement data is always uniform and without pop-in; the contrast between these regions is shown in Fig. 3(b), where higher hardness areas have increasingly steep load versus displacement curves, and the lowest measured hardness shows the pop-in phenomenon. The load versus displacement curve for the fused silica standard is provided for comparison. The large distribution in hardness is also associated with a wide range of Ta:B atomic composition as measured by XPS survey scans at several locations on the sample surface. Figure 4 shows XPS survey scans from sample C demonstrating the variation in Ta:B stoichiometry from two such locations. The Ta:B stoichiometry of nearly 1:1 (TaB) and 1:2 (TaB₂) is apparent. These data support the model of an inhomogenous distribution of boride precipitates near the surface, at least on the scale of XPS and nanoindentation surface probe volumes.

Previously reported hardness values for TaB₂ films grown via CVD have been measured at approximately 33 GPa [8]. We explain the higher hardness values measured in this study by considering the potential for combined influences from precipitation hardening (TaB₂ and TaB phases), solid solution hardening (primarily interstitial boron within BCC Ta), and compressive stress (primarily from the TaB₂ phase which presents itself more at higher temperature). In self-propagating high-temperature ball-milling experiments conducted with tantalum and boron powders, gradual decomposition of the solid solution occurs to form TaB and TaB₂ phases [20]. In that case, substitutional and interstitial solutions can be sustained within the tantalum structure, until it reaches critical values of 50 and 66% atomic boron,

corresponding to the TaB and TaB₂ precipitated phases, respectively. It is germane to point out that tantalum has been identified for its high solubility of interstitials and that in tantalum, properties such as hardness are highly influenced by the presence of interstitials [21].

For the MPCVD diffusion process, the concentration of boron is expected to decrease with depth into the substrate. SEM-energy dispersive spectroscopy (EDS) was performed on sample B, cross-sectioned to obtain line scan data (Supplementary material Fig. S1). The scan shows a gradual diffusion of boron into the substrate such that the EDS signal from B drops by about a factor of four from surface to bulk within a depth of several microns. Notably, the presence of other borides (Ta₂B and Ta₃B₄, etc.) are not found in XRD, possibly due to the stability of solid solutions except at the aforementioned atomic ratios. We propose that as boron diffuses into the substrate, a boron-rich layer dominated by TaB2 is created on the topmost surface, intermixed with a less-prominent TaB phase, along with a solid solution of boron in Ta that gradually becomes Ta-rich into the substrate. Intermixing of phases is supported by the nanoindentation data, which occasionally reveal the pop-in phenomena from softer regions during loading [22]. A schematic of this proposed mechanism/structure is given in Fig. 5.

Bias voltage variation

All biased samples (Table I, samples D–G) were grown in the temperature regime of 750–800 °C. Of these, only the lower bias samples (D and E) resulted in little to no discrete boron-rich dark coating. However, the discrete coating reappeared at higher voltages, likely due to the effect of high DC bias. As reported elsewhere [23], the microwave discharge is enhanced at the edges of the substrate in the presence of a DC bias. For the samples processed at lower DC bias (samples D and E), either no coating was observed or the coating was distributed on the sample without any discernible pattern. However, when the bias voltage is increased to -250 V (sample F), a clear coating in the shape of an annular ring emerges near the edges. This ring persists on sample G (-350 V) with a boron-rich coating forming near the

^aFrom Highscore database ICSD database FIZ Karlsruhe 2017-1.



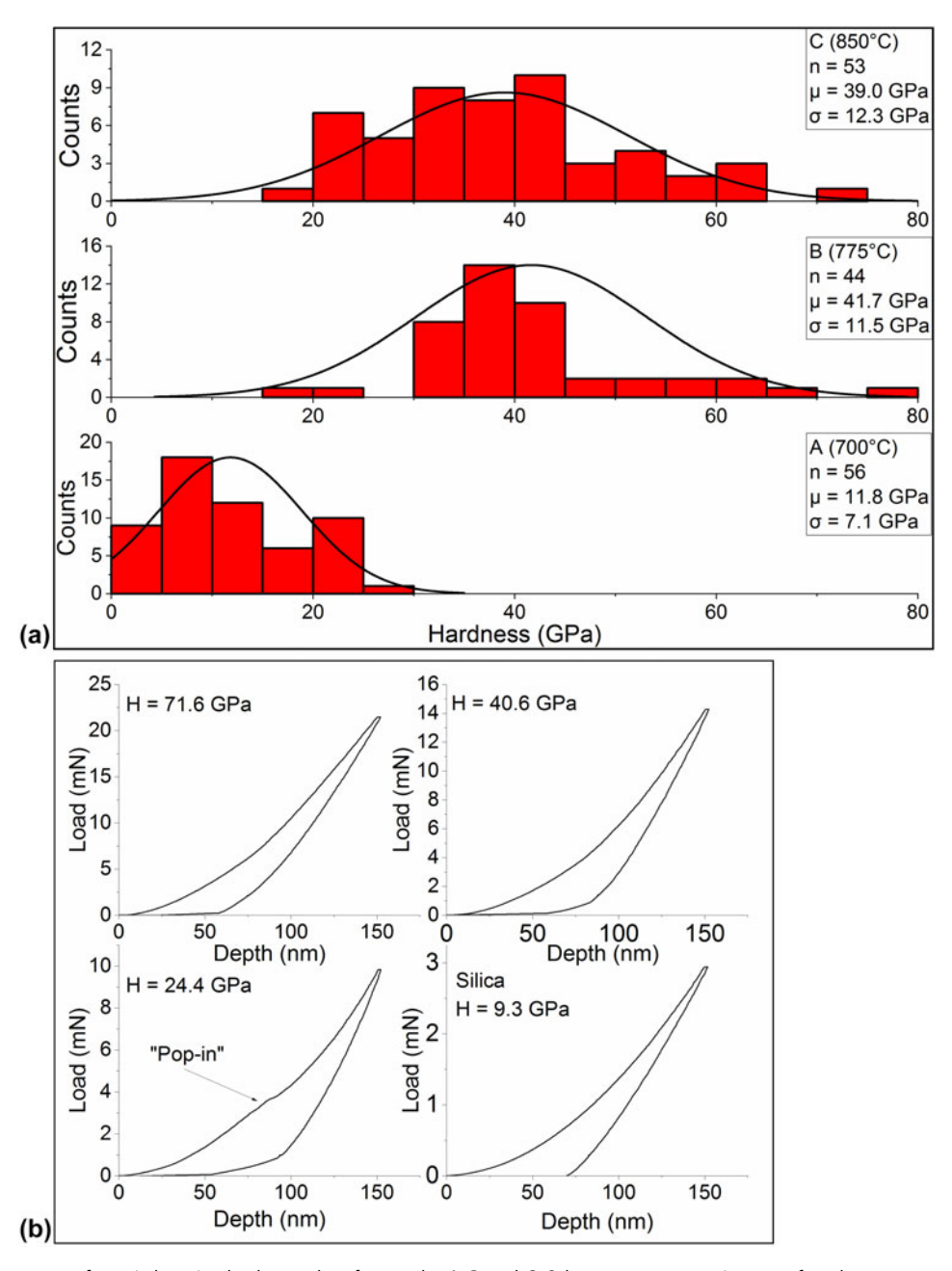


Figure 3: (a) Histograms of nanoindentation hardness values for samples A, B, and C. Substrate temperature increases from bottom to top. (b) Load versus displacement curves for different regions on sample C (850 °C), with a "pop-in" event shown.

edge that gradually becomes more metallic in appearance toward the center. As observed for the samples made at different temperatures (A–C), the pyrometer temperature profiles for samples F and G showed oscillations due to this coating.

Unlike the apparent proportional trend between temperature and relative intensity of TaB₂ shown in Fig. 3(a), the XRD profiles for samples D–G, presented in Fig. 6, are not as straightforward. While samples D and G show a very strong TaB₂ signal, sample E shows more intense Ta and TaB peaks. For sample F, the Ta signal is significantly more intense than

either TaB or TaB₂. As with the temperature set, a Reitveld fit was used to find the lattice parameters, as shown in Table II. Samples E and F (which show Ta signals in the XRD pattern) reveal an increase in Ta unit cell volume, again consistent with higher boron diffusion into the lattice that likely forms a solid solution. The resulting lattice strain is measured to be 0.26% for sample E and 0.33% for sample F. Given the measured Young's modulus for bare tantalum metal of 190 GPa, the calculated tensile stress in the tantalum is 0.50 GPa (sample E) and 0.62 GPa (sample F).



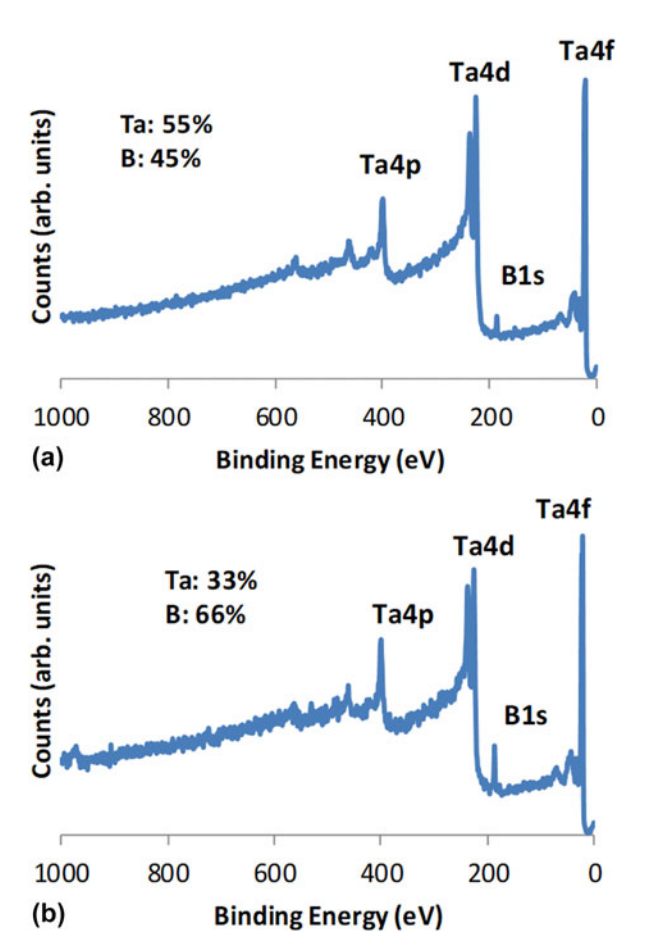


Figure 4: XPS survey scans showing variation in composition on the sample C surface. The compositions are associated with Ta:B stoichiometry of nearly 1:1 and 1:2, respectively.

Some insight into the trend in XRD patterns may come from the in situ OES data. The intensity ratio of the atomic boron emission (249 nm) to the hydrogen Balmer emission H_{α} (656 nm) remains relatively constant for the first three voltages tested, but then increases by a factor of approximately three at -350 V (Supplementary material Fig. S2). Reports for CVD diamond growth describe changes in OES carbon species including CH (387.5 nm and 430.9 nm), CH⁺ (423.9 nm), and C₂ (516.3 nm) with varying DC bias [24]. The use of electrical bias has also been found to increase ion bombardment of the substrate surface [24], which may, under some conditions, have the effect of etching the surface. Our observed change in XRD patterns could be explained due to surface etching with increasing bias, such that the surface-level boron is being preferentially etched away. This may be such that the tantalum-toboron ratios needed to precipitate crystalline borides are less likely to be created throughout the diffused volume and more likely to remain mixed as a solid solution. This can be seen by the general increase of the tantalum peak intensity between scans D, E, and F, by the increase in the TaB peak intensity from D to E, and by its decrease from E to F. For -350 V bias, the amount of boron in the chamber may be high enough to overcome the etching effect, resulting in the observed intense TaB₂ and TaB XRD reflections.

Support for this hypothesis comes from the nanoindentation data for the biased samples, shown in Fig. 7. For comparison, sample B (no bias) is included because its average temperature was in the same region as the biased samples. At -50 V, the etching effect would be low enough that the formation of borides is not inhibited, leading to hardness values that are comparable to sample B. For samples E and F, the effect of etching would be such that less borides are precipitated and the distribution of hardness is spread to lower values. This corroborates the XRD patterns for these samples, which show lower relative boride formation. For sample F, many of the lower hardness values were found closer to the edge of the sample-where the plasma is enhanced by the bias-indicating that the etching from ion bombardment was increased in this region. Finally, sample G with its higher plasma emission from atomic boron is able to overcome the etching effect enough to effectively precipitate the borides, particularly the TaB₂ phase.

Figure 8(a) is a bright field (BF) transmission electron microscopy (TEM) micrograph from sample C revealing the columnar grain morphology of the film. A magnified region, labeled I, within this microstructure is shown in Fig. 8(b). The selected area diffraction pattern, Fig. 8(c), from the region marked II, Fig. 8(b), confirms the prior TaB2 XRD results. A larger selected area diffraction pattern that captures both this phase and more of the surrounding region is shown in Fig. 8(d). If one compares the two diffraction patterns, using the dashed circle that is around the (001) TaB₂ reflection as a reference, additional reflections are noted. A dark field (DF) image, Fig. 8(e), from this pattern reveals the spatial location and size of a phase that is not in region II. This DF image is formed from the reflection noted by the solid white circle in Fig. 8(d). This particular reflection can be indexed to either the (101) TaB2 or (111) TaB plane based upon their similar interplanar spacing. Since this circled reflection was absent in the selected area pattern for the TaB2 phase shown in Fig. 8(c), and no other additional reflections for the (001) TaB phase now appear in the pattern shown in Fig. 8(d), it is suspected to be the TaB phase, which again would be consistent with the XRD phase identification for the twophase mixture. Furthermore, a closer examination of Fig. 8(a) reveals distinct contrast in the microstructure between different regions, with the clearly identified TaB2 region appearing as a continuous, dark gray contrast in the columnar grain morphology.

Downloaded from https://www.cambridge.org/core. IP address: 24.96.9.145, on 07 Apr 2020 at 20:06:57, subject to the Cambridge Core terms of use, available at https://www.cambridge.org/core/terms. https://doi.org/10.1557/jmr.2019.357



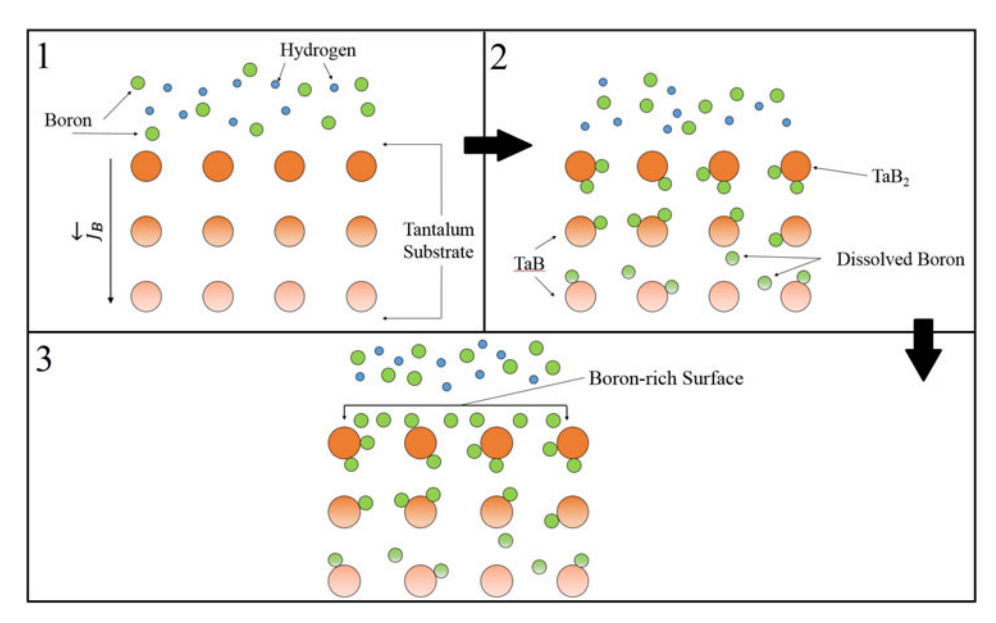


Figure 5: Schematic depicting the proposed diffusion process. Note the formation of the boron-rich coating on top of the surface after the surface becomes saturated with boron.

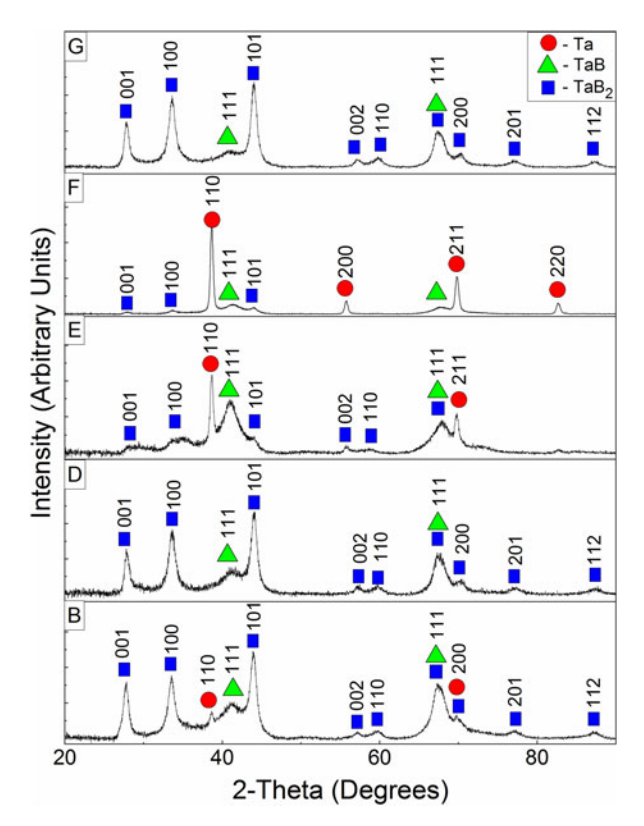


Figure 6: The XRD patterns for voltages ranging from 0 V to -350 V.

Conclusions

The effectiveness of the MPCVD process in boriding tantalum was investigated in this study, through a study of two growth conditions: the substrate temperature and

substrate bias. The temperature range was from 700 to 850 °C, and the bias magnitudes ranged from -50 to -350V. XRD patterns show a clear increase in the relative intensity of the TaB2 phase with temperature, accompanied by an increase in hardness measured via nanoindentation. An average hardness value for samples with significant TaB2 XRD signals was approximately 40 GPa, with values as high as 75 GPa. In addition to the formation of nanoscale borides, we propose that the MPCVD process also forms interstitial and substitutional solid solutions of boron in tantalum. This is based on previous literature findings and is consistent with a diffusionassisted process. We suggest that the combined effect of these phases, in addition to compressive stress in the borides, presents localized surface regions having superhardness (>40 GPa). Implementation of a substrate bias did not further increase hardness. In fact, the XRD and nanoindentation data show that for the midrange bias values used, a decrease in the amount of desired boride phases with subsequent lower measured hardness was observed. A competition between bias-induced etching of the substrate at low midrange voltages and an increase in atomic boron emission that promotes boride precipitation at high bias voltages may explain the measured XRD and nanoindentation data.

Future work in this area could focus on improving the homogeneity of the boride layer. Additionally, the etching effect caused by application of substrate bias may be mitigated by plasma boriding without bias, and only then turning it on once, a sufficiently thick boride layer is formed. This may then allow hardening from ion bombardment without undesirable

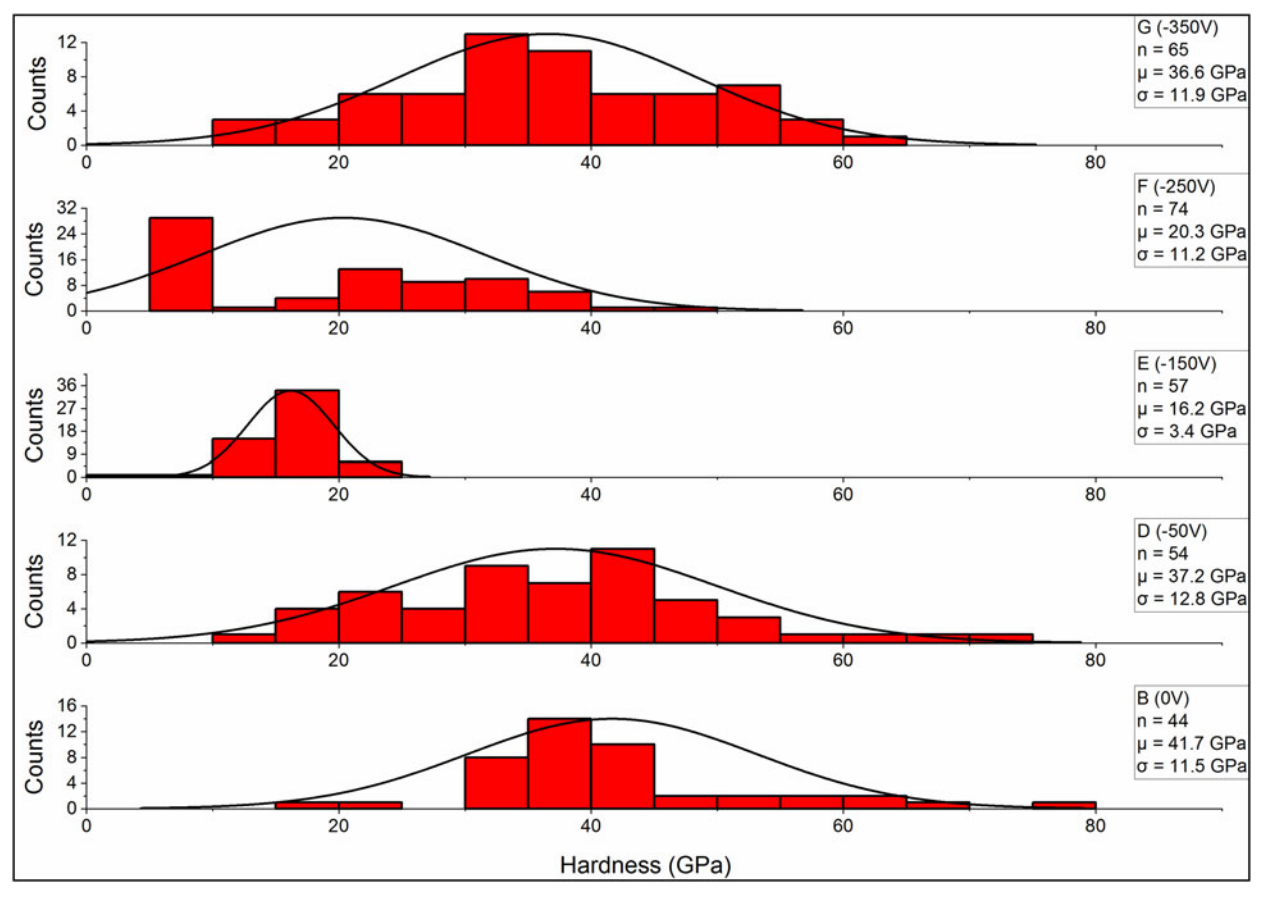


Figure 7: Histograms of nanoindentation hardness for samples C-G; bias voltage increases in magnitude from bottom to top.

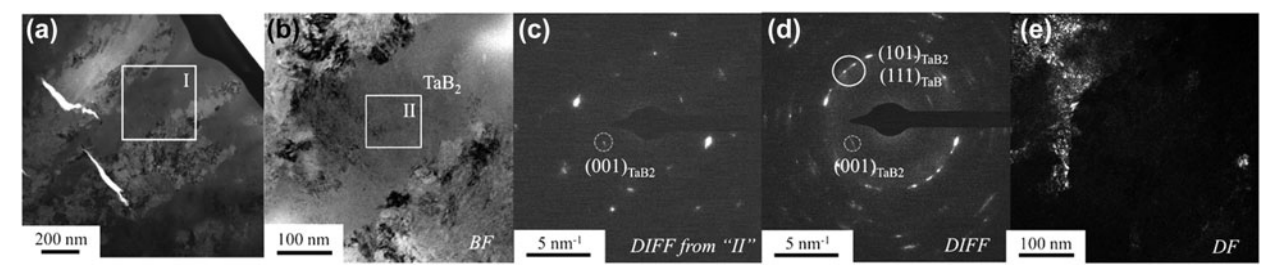


Figure 8: (a) BF image of sample C revealing the columnar grain morphology. (b) Magnified region I shown in (a). (c) Selected diffraction area pattern from region Il shown in (b) with the reflections confirming the TaB2 phase. (d) Selected diffraction area pattern from (b). (e) Dark field image from the identified reflection circled by the solid circle in (d).

etching effects. Finally, mechanical integrity (e.g., fracture toughness) of the borided surface should be evaluated.

Methods

Downloaded from https://www.cambridge.org/core. IP address: 24.96.9.145, on 07 Apr 2020 at 20:06:57, subject to the Cambridge Core terms of use, available at https://www.cambridge.org/core/terms. https://doi.org/10.1557/jmr.2019.35

The tantalum substrates (99.98% purity; Source: ESPI Metals, Ashland, Oregon) were 8-mm diameter disks of thickness 0.51 mm cut from a rectangular stock. Samples were ground with progressively finer grits of silicon carbide paper (ANSI 120 to 1200) and then polished with diamond-charged cloths (9 μm-1 μm particle size). A final polish was done using colloidal silica suspension. Samples were then cleaned with acetone, methanol, and distilled water to remove any residual debris.

A diagram of the MPCVD reactor (WaveMat MPDR 313EHP, Plymouth, Michigan) used in this study is provided in the Supplementary material (Fig. S3). The Ta substrates were placed on a molybdenum screw centered on a water-cooled stage positioned into the upper chamber of the reactor. For all experiments, the flow rate of H₂ gas was 500 sccm and the chamber pressure was 15 torr. The flow rate of diborane (B₂H₆) was 0.6 ± 0.15 sccm (with uncertainty due to low flow-rate



accuracy limits of the mass flow controller). A summary of sample parameters is given in Table I. Substrate temperature was measured using a Mikron (Model M77) two-color infrared pyrometer. Additionally, an optical fiber (200 \pm 5 μm core diameter, 0.22 \pm 0.02 numerical aperture) was used to collect plasma emission for OES analysis. OES data were taken with an Acton Research Spectra Pro 500i spectrograph (Princeton Instruments, Trenton, New Jersey), entrance slit set at 20 μm , and a 1200-g/mm grating blazed at 300 nm.

The first set of experiments involved varying the substrate temperature with no bias applied; the three target growth temperatures tested were 700, 775, and 850 °C. Variation of microwave power was used to achieve these three temperatures, as shown in Table I.

The second set of experiments involved applying a negative bias to the substrate. In these experiments, the microwave power was fixed at 600 W, resulting in an average substrate temperature between 750 and 800 °C. The bias voltages tested were -50 V, -150 V, -250 V, and -350 V. The bias voltage was provided by a Sorensen DCS 600-1.7E power supply. The negative terminal was connected to the molybdenum screw (on top of which the substrate was placed), and the ground connection was placed on the outer side of the reactor. In this way, the sample was biased relative to the walls of the chamber.

Hardness was measured using an MTS NanoIndenter XP with a Berkovich diamond tip (nominal radius 50 nm). Calibration of the indenter area function before and after hardness measurements was tested for the fused silica standard (accepted Young's modulus of 72 GPa) to confirm that the tip geometry did not change during testing of all samples. All indents, including those on silica, were made to a maximum depth of 150 nm. The measured hardness was determined at maximum load. The range of before/after measured silica Young's modulus values (73.5 \pm 3.6 GPa) was found to be consistent with the accepted value; therefore, the indenter tip area function was determined not to have changed significantly during testing.

Additional analysis and characterization of samples included XPS, XRD, SEM, and TEM. The XPS instrument used was a Phi Electronics Versaprobe 5000. Survey scans were performed using a conventional Mg source. A focused Al monochromatic source was used when Ar-ion sputtering was needed to remove surface contamination. The XRD machine was a PANalytical Empyrean X-ray diffractometer with Cu K_{α} anode ($\lambda=1.54158$ Å) with a 1/8th-inch divergence slit, and a 1/16th-inch antiscatter slit. XRD patterns were analyzed using the HighScore software, version 4.8. A glancing-angle XRD scan with an incident angle of 1° was performed for phase identification. SEM imaging was performed with a FEI QuantaTM 650 FEG at 10-kV beam voltage. Furthermore, data from the pyrometer and OES probe were analyzed in a custom program written in MATLAB by the

authors. The lamella for the TEM study was prepared by a site-specific lift-out procedure using focused ion beam (FIB) in Tescan Lyra dual beam FEG FIB. The lamella was thinned to a thickness of approximately 100 nm using 30 kV ion beam. Subsequent low-voltage (5 kV) milling steps were carried out to reduce the FIB-damage. The TEM sample was analyzed with BF, DF, and selected area electron diffraction (SAED) modes using a FEI Tecnai G20 TEM operated at 200 kV.

Acknowledgments

Support provided by the National Aeronautics and Space Administration (NASA)-Alabama Space Grant Consortium, Research Experiences for Undergraduates (REU) award to University of Alabama—Birmingham (UAB). This material is also based upon work supported by the National Science Foundation (NSF) EPSCoR RII-Track-1 Cooperative Agreement OIA-1655280. We also acknowledge support from the NSF Major Research Instrumentation (MRI) Grant No. DMR-1725016. Any opinions, findings, and conclusions or recommendations expressed in this material are those of the authors and do not necessarily reflect the views of the National Science Foundation. The authors also thank Bernabe S. Tucker for assistance with SEM imaging.

Supplementary material

To view supplementary material for this article, please visit https://doi.org/10.1557/jmr.2019.357.

References

- S. Carenco, D. Portehault, C. Boissière, N. Mézailles, and
 C. Sanchez: Nanoscaled metal borides and phosphides: Recent developments and perspectives. *Chem. Rev.* 113, 7981–8065 (2013).
- E. Medvedovski, F.A. Chinski, and J. Stewart: Wear- and corrosion-resistant boride-based coatings obtained through thermal diffusion CVD processing. *Adv. Eng. Mater.* 16, 713–728 (2014).
- **3. X. Zhang, E. Zhou, and Z. Wu**: Prediction of a new high pressure phase of TaB3: First principles. *J. Alloys Compd.* **632**, 37–43 (2015).
- S. Okada, K. Kudou, I. Higashi, and T. Lundström: Single crystals of TaB, Ta₅B₆, Ta₃B₄, and TaB₂, as obtained from high-temperature metal solutions, and their properties. *J. Cryst. Growth* 128, 1120–1124 (1993).
- Y. Dzyadykevych and O. Smiyan: Investigation of the initial stage of borating tantalum. Int. J. Refract. Met. Hard Mater. 25, 361–366 (2007).
- 6. A. Friedrich, B. Winkler, E.A. Juarez-Arellano, and L. Bayarjargal: Synthesis of binary transition metal nitrides, carbides and borides from the elements in the laser-heated diamond anvil cell and their structure-property relations. *Materials* 4, 1648–1692 (2011).

© Materials Research Society 2019 cambridge.org/JMR



- H. Chen, H. Liang, L. Liu, H. Li, K. Liu, and F. Peng: Hardness measurements for high-pressure prepared TaB and nano-TaC ceramics. *Results Phys.* 7, 3859–3862 (2017).
- S. Motojima, K. Kito, and K. Sugiyama: Low-temperature deposition of TaB and TaB₂ by chemical vapor deposition. *J. Nucl. Mater.* 105, 262–268 (1982).
- J.A. Mugabi: The Chemical Vapour Deposition of Tantalum—In Long Narrow Channels (Department of Energy Conversion and Storage, Technical University of Denmark, 2014). Available at: https://orbit.dtu.dk/files/104276111/
 THE_CHEMICAL_VAPOUR.pdf (accessed July 26, 2019).
- J. Johnston, M. Jubinsky, and S.A. Catledge: Plasma boriding of a cobalt-chromium alloy as an interlayer for nanostructured diamond growth. *Appl. Surf. Sci.* 328, 133–139 (2015).
- J. Johnston and S.A. Catledge: Metal-boride phase formation on tungsten carbide (WC-Co) during microwave plasma chemical vapor deposition. *Appl. Surf. Sci.* 364, 315–321 (2016).
- J. Ballinger and S.A. Catledge: Metal-boride interlayers for chemical vapor deposited nanostructured NSD films on 316 and 440C. Surf. Coat. Technol. 261, 244–252 (2015).
- X. Chen, H. Gao, Y. Bai, and H. Yang: Thermal failure mechanism of multilayer brittle TiN/CrAlN films. *Ceram. Int.* 44, 8138–8144 (2018).
- X. Chen, X. Pang, J. Meng, and H. Yang: Thermal-induced blister cracking behavior of annealed sandwich-structured TiN/CrAlN films. Ceram. Int. 44, 5874–5879 (2018).
- 15. X. Chen, Y. Xi, J. Meng, X. Pang, and H. Yang: Effects of substrate bias voltage on mechanical properties and tribological behaviors of RF sputtered multilayer TiN/CrAlN films. *J. Alloys Compd.* 665, 210–217 (2016).
- **16. D. Kang, S. Ha, and K. Kim**: Evaluation of the ion bombardment energy for growing diamondlike carbon films in an electron

- cyclotron resonance plasma enhanced chemical vapor deposition. J. Vac. Sci. Technol., A 16, 2625–2631 (1998).
- 17. Z.L. Akkerman, Y. Song, Z. Yin, and F.W. Smith: In situ determination for the surface roughness of diamond films using optical pyrometry. *Appl. Phys. Lett.* 72, 903–905 (1998).
- 18. J.W. Ager, III and M.D. Drory: Quantitative measurement of residual biaxial stress by Raman spectroscopy in diamond grown on a Ti alloy by chemical vapor deposition. *Phys. Rev. B* 48, 2601– 2607 (1993).
- P. Scardi, M. Leoni, G. Cappuccio, V. Sessa, and M.L. Terranova: Residual stress in polycrystalline diamond/Ti-6Al-4V systems. *Diamond Relat. Mater.* 6, 807–811 (1997).
- 20. M.P. Savyak, O.B. Melnick, M.A. Vasil'kivska, I.I. Timofeeva, V.I. Ivchenko, and I.V. Uvarova: Mechanical synthesis of tantalum borides and modeling of solid solutions of boron in tantalum. *Powder Metall. Met. Ceram.* 57, 373–383 (2018).
- 21. G. Marinelli, F. Martina, S. Ganguly, and S. Williams: Microstructure, hardness and mechanical properties of two different unalloyed tantalum wires deposited via wire + arc additive manufacture. *Int. J. Refract. Met. Hard Mater.* 83, 104974 (2019).
- S.V. Hainsworth, H.W. Chandler, and T.F. Page: Analysis of nanoindentation load-displacement loading curves. *J. Mater. Res.* 11, 1987–1995 (1996).
- 23. S. Barrat, S. Saada, I. Dieguez, and E. Bauer-Grosse: Diamond deposition by chemical vapor deposition process: Study of the bias enhanced nucleation step. J. Appl. Phys. 84, 1870–1880 (1998).
- 24. H.C. Barshilia, B.R. Mehta, and V.D. Vankar: Optical emission spectroscopy during the bias-enhanced nucleation of diamond microcrystals by microwave plasma chemical vapor deposition process. J. Mater. Res. 11, 2852–2860 (1996).